INTERNATIONAL JOURNAL OF AUTOMOTIVE AND MECHANICAL ENGINEERING (IJAME)
ISSN: 2229-8649 e-ISSN: 2180-1606
VOL. 19, ISSUE 3, 9950 – 9963
DOI: https://doi.org/10.15282/ijame.19.3.2022.07.0767

ORIGINAL ARTICLE

Machinability Study on AA6061/2 SiC / Graphite Hybrid Nanocomposites Fabricated through Ultrasonic Assisted Stir Casting

Virinchi Krishna Lagisetti[1,*], A. Prasad Reddy[1], Chamaiporn Sukjamsri[2], and P. Vamsi Krishna[1]

[1]Department of Mechanical Engineering, N.I.T Warangal, Warangal 506004, Telangana, India.
[2]Department of Biomedical Engineering, Srinakharinwirot University, 26120 Nakhon Nayok, Thailand.

ABSTRACT – Aluminium-based hybrid metal matrix nanocomposites (AA-HMNCs) have numerous applications due to their higher strength-to-weight ratio and good mechanical and tribological properties. However, the machinability aspect of these materials must be carefully explored before employing them in various engineering applications. The present study involves the fabrication of AA6061/2 wt.% SiC/x wt.% graphite (x= 1, 2, 3) hybrid nanocomposites and subsequently subjecting them to machinability investigation. All the hybrid nanocomposite samples are fabricated through ultrasonic assisted stir casting technique. The effect of machining parameters and graphite content of the sample on cutting force and surface roughness is discussed based on experimental data. Experiments are performed based on the central composite design of response surface methodology, and the corresponding output responses are recorded. ANOVA analysis revealed that the graphite content has the highest authority over surface roughness and cutting force. High cutting speeds accompanied by low feed and depth of cut have resulted in reduced cutting forces and better surface finish. Chip morphology studies have also subsequently indicated better machinability with increased graphite content.

ARTICLE HISTORY
Received: 17th Jan 2022
Revised: 15th Aug 2022
Accepted: 10th Sept 2022
Published: 30th Sept 2022

KEYWORDS
Hybrid nanocomposite;
Silicon carbide;
Graphite;
Turning;
Machinability

INTRODUCTION

The current world of engineering applications requires materials that offer high strength, less weight, good mechanical and tribological properties. Aluminium-based Metal Matrix Nanocomposites (MMNC) belong to such a class of materials due to their strength, wear resistance, and stiffness. However, the extent of material properties depends on the size and type of reinforcement used in addition to the fabrication method employed. AA6061 is one of the aluminium alloys that is widely employed in a variety of applications. Ultrasonic-assisted stir casting is one of the widely employed fabrication techniques for making MMNC. It has successfully demonstrated its ability to disperse the nano reinforcement particles uniformly by greatly limiting any agglomerations [1]. Adding more than one reinforcement material to the matrix will often result in the manifestation of some useful traits. Such a class of composite materials is called hybrid composites. Silicon carbide (SiC) is a popular choice as reinforcement for aluminium-based MMNC due to its hardness and wear resistance [2]. Graphite is also a suitable reinforcement for aluminium MMNC since it increases the tensile strength of the material [3]. It inherently becomes desirable that the materials used for engineering applications can be machined easily. As aluminium MMNCs gained popularity, it became the need of the hour to investigate the machinability aspects of these materials. The current study investigates the machinability aspects of the aluminium alloy-SiC-graphite hybrid nanocomposites.

Vinoth et al. [4] synthesized an Al 7075 / SiC composite via stir casting. Microstructure analysis conveyed that reinforcement particles were distributed uniformly since stir casting was chosen as the method of fabrication. Yadav et al. [5] reviewed the works on stir-casted aluminium metal matrix composites. Apparently, the inclusion of SiC as the reinforcement material resulted in improved mechanical properties. Narayana et al. [6] studied the effect of graphite on stir-casted aluminium metal matrix composites. The selection of graphite as reinforcement has led to a reduction in material hardness. Kannan et al. [7] made a contrast of both microstructural and mechanical properties for AA 7075-based nanocomposite of 2 wt.% nano alumina particles and hybrid nanocomposites having 4 wt.% SiC along with two different weight fractions of nano alumina particles, fabricated via stir casting and squeeze casting. It was reported that a weight fraction not exceeding 2 wt.% leads to uniform distribution of nano reinforcement particles without any cluster formation.

Prasad et al. [8] conducted studies on the dry sliding behavior of AA6061/SiCp nanocomposites produced using ultrasonically assisted stir casting. It was concluded that the nanocomposites improved their wear resistance due to the rise in SiCp content. The coefficient of friction was also reportedly increased due to the rise in SiCp content. Sridhar et al. [9] studied wear aspects of Al 7075-Silicon carbide-graphite hybrid composite. Graphite presence has reportedly improved the wear resistance of the material. Prasad et al. [10] performed studies on the tribological behavior of Al 6061 based hybrid nanocomposite with reinforcements including 2 wt.% SiC and graphite nanoparticles of varied weight fractions. A trend of decreasing coefficient of friction was reported due to a rise in graphite content, with the decrement

*CORRESPONDING AUTHOR | Virinchi Krishna Lagisetti | ✉ iamvirinchikrishna@gmail.com

peaking at 2 wt.% concentration. Senthilkumar et al. [11] noticed that the hardness of the hybrid aluminium composite would increase with the rise in SiC content and decrease by increasing the graphite content.

Chen et al. [12] reviewed the machinability aspects of silicon carbide particle (SiC-p) reinforced aluminium composites. Abrasion caused by reinforcement particles is found to be responsible for tool wear during the machining operation. Moreover, the higher the concentration of SiC, the greater would be the tool wear. Ozben et al. [13] conducted experiments on the machinability of SiC-p reinforced aluminium MMC with the concentration of reinforcement as 5, 10, and 15 wt.%. Reportedly higher SiC content resulted in increased tool flank wear along with adverse effects on the surface roughness. Harish et al. [14] discussed that the machining of Al/SiC MMC has its own set of challenges to overcome. SiC particles, despite making the MMC hard, would also act as a cutting edge when machined upon. Poor surface finish and low machining rate are the problems that are often associated with the machining of aluminium–silicon carbide MMC. Deshmukh et al. [15] reviewed aluminium metal matrix composites. Tool wear during turning aluminium matrix composites was dependent on cutting velocity with type and amount of reinforcement used. Venkatesan et al. [16] investigated the cutting forces encountered and also the surface roughness obtained while machining Al 356/SiC/B4C hybrid composite. High SiC content has led to deteriorated surface finish and increased cutting forces. Kannan et al. [17] evaluated surface roughness and cutting forces encountered while performing turning operation on Al 7075-silicon carbide-graphite hybrid composite. The study reported better surface finish, low tool wear, and reduced cutting forces with the rise in graphite content. Suthar et al. [18] suggested that the combination of optimum cutting parameters and the type of reinforcement used would decide the surface finish of the aluminium hybrid composites under machining. Increased graphite content in the composite also reportedly led to low surface roughness.

Rohit and Onkar [19] conducted turning experiments on Al 6063 using a CNC machine. With the Taguchi L_{27} technique, the study explored surface roughness and its dependency on cutting parameters such as spindle speed, feed, and depth of cut. It was concluded through ANOVA that feed was more significant on the surface roughness among all other parameters. Kilickap et al. [20] implemented the Taguchi technique along with response surface methodology (RSM) to reduce the burr height and surface roughness during the drilling operation on Al-7075 alloy. It was found that the experimental values and predicted values from the RSM model are almost close. Thakre and Soni [21] studied the burr formation while drilling an Al6061-SiC MMC through a model developed using RSM. The conclusions from the ANOVA test elucidated that both feed rate and drill point angle are essential for minimizing the burr height. Thiagarajan and Kayaroganam [22] implemented a central composite design (CCD) for optimizing the machining parameters for drilling hybrid MMCs. Their investigation has concluded that the implementation of CCD was instrumental in predicting burr height, thrust and surface roughness with the help of mathematical models. A similar conclusion was drawn by the study conducted by David et al. [23]. However, this investigation employed an RSM with a four-factor CCD based experimental design.

While there are several studies on aluminium matrix hybrid composites, the ones that deal with their machinability aspects are limited in number. Moreover, machinability studies on AA6061/SiC/graphite composites are mostly on the ones with relatively high amounts of micro-size SiC and graphite reinforcements. The present work proposes a relatively low nanosized SiC and graphite content for the ease of machinability. The current study mainly deals with examining the effect of cutting speed, depth of cut, feed rate, and graphite content on cutting force and surface roughness during machining of AA606/ 2 wt.% SiC/ x wt.% graphite (x= 1, 2, 3) hybrid metal matrix nanocomposites. The study also includes the analysis of chip morphology using a Scanning Electrode Microscope (SEM). Since the output parameters are heavily dependent on the input variables, it becomes imperative to adopt an effective experimental design for achieving accurate and reliable results. It is a well-known fact that RSM-based experimental design has yielded not only better results but also crisp and accurate experimental trials. Even the studies reviewed in the literature have emphasized the significance of RSM-based design. Hence, the current investigation employs the RSM technique for designing the experiments. The outputs from the experiments are used for developing the polynomial regression equations for cutting forces and surface roughness in terms of input process parameters. Based on the influence that the input parameters hold on cutting force and surface roughness, optimum values of input parameters are identified for improving the machining performance. The current study focuses on optimizing the cutting forces and surface roughness in machining of AA6061-2 wt.% SiC – x wt.% graphite (x= 1, 2, 3) hybrid nanocomposite using Response Surface Methodology (RSM).

The remainder of this paper is organized as follows: Section 2 briefly presents an overview of material selection and methodology adopted for the study. Section 3 provides the results obtained from the experiments along with a discussion on them. Section 4 concludes the paper.

MATERIALS AND METHODS

AA6061, an aluminium wrought alloy, was chosen as the matrix material based on the benefits it can offer [15]. It was supplied by Bharat Aerospace Metals, India, in the form of a commercial ingot. The ingot was procured in T6 condition and had a nominal composition of Mg-0.93 %, Si-0.52 %, Fe-0.25 %, Cu-0.18 %, Mn-0.14 %, Zn-0.09 %, Cr-0.07 %, Ni-0.03 %, Ti-0.01 %, and the balance being aluminium. The beta-phased silicon carbide nanoparticles (SiCp) and graphite nanoparticles are chosen as particulate type reinforcements in the fabrication of Hybrid Metal Matrix Nano Composites (HMMNC). Table 1 showcases the details related to all the constituent materials. Silicon carbide was found to possess cubic morphology and was fabricated using the plasma chemical vapor deposition technique. All the constituents discussed above for manufacturing the hybrid nanocomposite can be seen as displayed in Figure 1.

Table 1. Details of AA6061 aluminium alloy, β-SiCp and graphite nano-reinforcements particles.

Material	Hardness (GPa)	Average particle size (nm)	Density (gm/cm^3)	Melting point (^{o}C)
AA6061 alloy		-	2.7	650
β-SiCp	24.5 – 28	50	3.218	2730
Graphite	0.25	500	2.266	3730

(a) (b) (c)

Figure 1. Constituents of nanocomposite: (a) AA6061 aluminium alloy (b) β-SiCp and (c) graphite.

Regardless of the type of fabrication process, the presence of moisture in the alloy matrix and the distribution of the reinforcing materials are key issues to be addressed. Although several methods have been proposed to overcome these issues, ultrasonic-assisted stir casting is chosen to be the fabrication methodology. The experimental setup of the technique is shown in Figure 2. This method is also suitable for manufacturing MMNCs comprising alloys of cast Al, and SiC. Ultrasonic-assisted casting integrates the curing process with nanoparticle dispersion by ultrasonic cavitation in the molten metal. Since the nanoparticle clusters are loosely packed for collection, there is a possibility of entrapment of air in the voids of the clusters. The size of the cluster varies from nanometre to micrometer due to the attractiveness of the nanoparticles and the low wettability between the nanoparticles and the molten metal. Ultrasonic cavitation can produce transient thermal micro-dots that can reach temperatures of about 5000°C, pressures of 1000 atm, and heating and cooling rates of over 1010 K / s. Strong local high-impact collisions can destroy clusters of nanoparticles and clean the surface of the particles. The experimental apparatus includes an oven, a control member, an ultrasonic generator with a transducer, a stirrer, a jig, a mould, and a furnace for heating the nanopowder.

Being the primary reinforcement, the quantity of SiC was decided as 2 wt. % as this composition is well dispersed in the matrix without any cluster formation [24]. Moreover, for retaining the maximum possible hardness without later compromising on machinability, SiC was restricted to 2 wt.%. The material samples are collectively represented as AA6061/2wt. % SiCp/x wt. % graphite (x = 1, 2, 3). Each sample is named 1HNC, 2HNC, and 3HNC based on the graphite percentage in them. All of them were fabricated using ultrasonically assisted stir casting in an inert atmosphere created by argon gas.

Figure 2. Experimental setup of ultrasonically assisted stir casting.

Nanoparticles of both reinforcements were kept in a folded aluminium foil which in turn is placed inside a muffle furnace for preheating them at 550ºC. At 780°C, the aluminium foil with reinforcement particles inside was fed into the AA6061 aluminium alloy melt. All three constituent materials would then be mixed with a mechanical stirrer for 10 minutes. A preheated ultrasonic probe coupled to a 20 kHz frequency ultrasonic generator of 2 kW power rating was employed. The probe was then positioned at a depth of 25 mm in the melt for 25 minutes. The ultrasonically processed molten composition would then be discharged into the mild steel mould, which was priorly heated to a temperature of 550°C. After solidification, the cast ones were removed from the die. The crucial components of the experimental setup can be shown individually, as displayed in Figure 3.

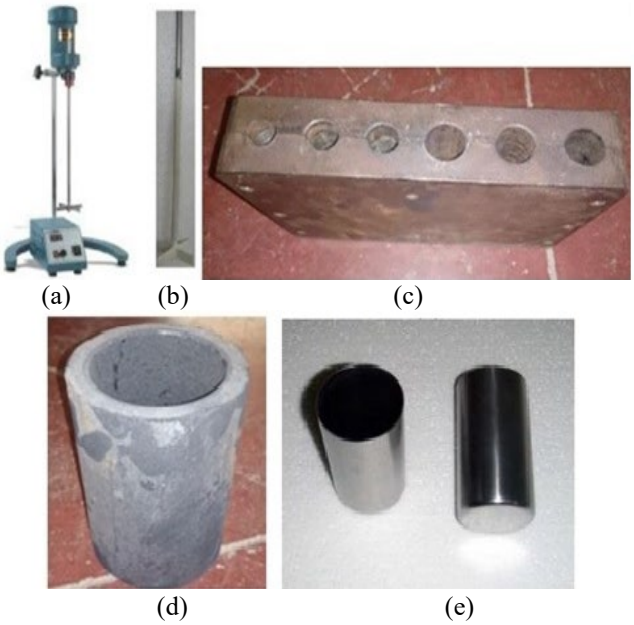

Figure 3. (a) Electromechanical stirrer (b) SS 304 stirrer rod coated with Zirconia (ZrO_2) (c) mild steel die (d) graphite crucible and (e) stainless steel crucible.

Central Composite Design (CCD) is adopted for performing the turning operations based on RSM based experimental design. In particular, face-centred CCD is considered since there is a three-level variation in all the factors. Parameters such as feed rate, cutting speed, depth of cut, and graphite wt.% are taken as control factors with three-level variations. Accordingly, we can arrive at the fact that there are eight axial points and six centre points in the design. All the factors considered in the design are continuous. A total of 30 experiments were carried out based on the CCD design for investigating the effect of input parameters on the output parameters such as cutting force and surface roughness. PCLNR 2525 M12 tool holder is used with CCMT 12 04 04 uncoated carbide tool insert for machining. Forces are measured using a piezoelectric dynamometer (Make: Kistler, Model: 5070) fitted at the bottom of the tool post. Measurement of surface roughness is accomplished offline post the turning operation using a portable roughness tester (Surtronic -S128). All the parameters needed for the experimentation, along with those of CCD are given in Table 2. ANOVA test was executed at a 95% confidence level on the obtained data of cutting forces and surface roughness to identify the most influencing parameter on the output variables. Figure 4 displays the hybrid nanocomposite samples after being taken out from the casting. The entire investigation can be summarized pictorially with the help of Figure 5, as it outlines the entire experimentation.

Table 2. Input parameters and their levels for the central composite design (CCD).

Specifications	Code	Low level-I (-1)	Medium level-II (0)	High level-III (+1)
Speed (m/min	A	50	75	100
Depth of cut (mm)	B	0.3	0.6	0.9
Feed rate (mm/rev)	C	0.05	0.10	0.15
AA6061-2SiC-Gx (Graphite)	D	(x = 1)	(x = 2)	(x = 3)
Cutting condition	--	Dry	Dry	Dry
Tool holder	MODEL (PCLNR 2525 M12)			
Tool geometry	Orthogonal Rake angle = -6º Clearance angle = 7º ; Inclination angle = -6º ; Approach angle = 95º ; Corner Radius = 0.4 mm			

Figure 4. HNC samples after casting.

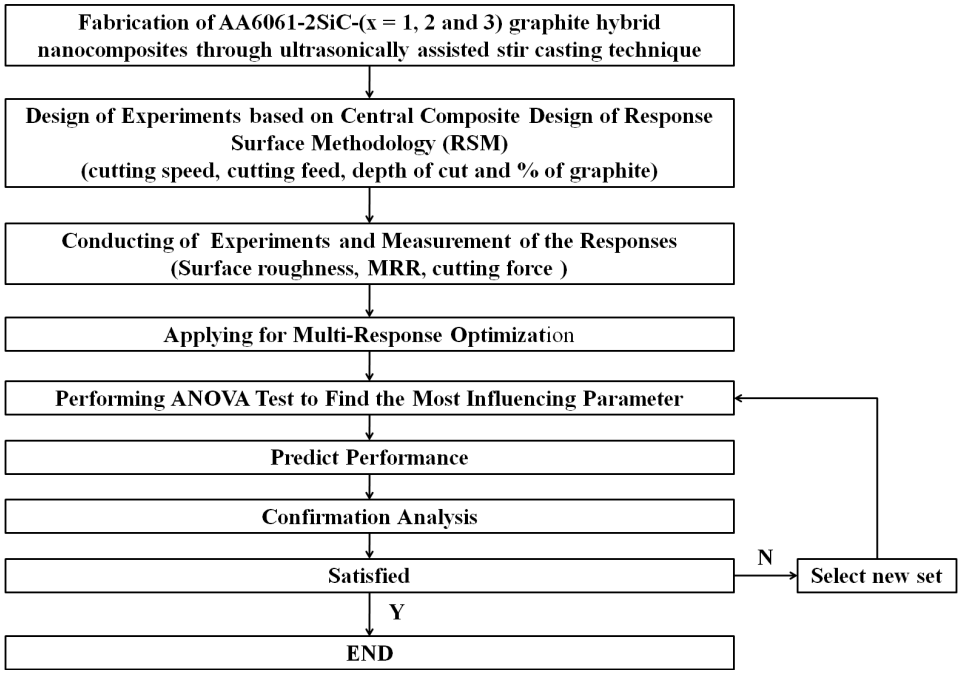

Figure 5. Structural outline of the investigation.

RESULTS AND DISCUSSION

The data obtained from the machining operation consisting of machining parameters with the corresponding output responses such as cutting force and surface roughness are tabulated in Table 3. The developed mathematical models have been analyzed at a 95% confidence level using the ANOVA technique. Tables 4 and 5 showcase the ANOVA results for cutting force and surface roughness respectively. The regression model test, model coefficients test, and lack-of-fit test have also been performed. Preliminary observations concerning the patterns visible in Table 3 suggest that feed and depth of cut have a significant effect on the cutting force rather than the cutting speed. Though very few instances report a reduction in cutting force at higher cutting speeds, in the overall scheme of things, feed and depth of cut emerge as the dominating factors. This is even more apparent from the fact that the lowest cutting force is a result of employing a combination of high cutting speeds with low feed and depth of cut. This discussion can be successfully extended to surface roughness as well. Both feed and depth of cut seem to be inversely proportional to surface roughness. The results in Table 3 provide ample evidence for this observation. This is in resonance with an apparent fact that a combination of high feed and depth of cut resulted in the highest surface roughness value.

Table 4 presents the results obtained after performing the ANOVA analysis on the input parameters and their effect on cutting force. It is safe to say that all the input parameters are significant enough to have considerable influence on the cutting force based on their respective p-values. However, there are some instances such as two-way interaction and squared parameter values that proved to be insignificant. The conclusions drawn from Table 3 concerning cutting force seem to be in accordance with the corresponding ANOVA results as well. The table also concludes that our model holds good as the p-value for lack of fit is well more than 0.05 asserting the model's effectiveness. Similarly, Table 5 holds the ANOVA results of surface roughness and its influential parameters. Cutting force seems to be an insignificant factor relative to the rest of them. This is in line with the earlier discussion on the results obtained in Table 3. The model also holds good for surface roughness since the lack of fit hypothesis is proven wrong thanks to its large p-value.

Table 3. Experimental observations.

Exp. No.	A	B	C	D	Cutting force (N)	Surface roughness (μm)
1	50	0.9	0.15	1	158	1.57
2	100	0.3	0.05	3	95	0.75
3	75	0.6	0.10	2	147	1.32
4	50	0.3	0.15	1	185	1.37
5	50	0.9	0.05	3	136	1.26
6	100	0.3	0.15	3	157	0.92
7	50	0.3	0.05	3	142	1.23
8	75	0.6	0.10	2	146	1.42
9	75	0.6	0.10	2	149	1.38
10	100	0.3	0.05	1	90	1.40
11	50	0.9	0.05	1	198	1.55
12	100	0.9	0.05	1	163	1.63
13	50	0.9	0.15	3	99	1.03
14	100	0.3	0.15	1	151	1.54
15	100	0.9	0.15	3	159	1.21
16	50	0.3	0.15	3	149	1.03
17	100	0.9	0.05	3	139	1.11
18	75	0.6	0.10	2	145	1.43
19	100	0.9	0.15	1	181	1.98
20	50	0.3	0.05	1	179	1.35
21	50	0.6	0.10	2	138	1.23
22	75	0.6	0.10	2	129	1.32
23	75	1.2	0.10	2	130	1.83
24	100	0.6	0.10	2	125	1.29
25	75	0.6	0.10	3	115	1.02
26	75	0.6	0.20	2	164	1.30
27	75	0.6	0.05	2	131	1.17
28	75	0.6	0.10	1	140	1.49
29	75	0.3	0.10	2	125	1.22
30	75	0.6	0.10	2	131	1.29

Table 4. Analysis of Variance (ANOVA) of cutting force.

Source	Degrees of freedom	Adj SS	Adj MS	F-Value	P-Value	Note
Model	15	18412.4	1227.49	530.07	0.000	significant
Blocks	1	1109.9	1109.90	479.29	0.000	
Linear	4	5561.8	1390.45	600.44	0.000	
A	1	854.2	854.22	368.88	0.000	
B	1	472.3	472.25	203.93	0.000	
C	1	644.7	644.67	278.39	0.000	
D	1	3584.2	3584.22	1547.78	0.000	
Square	4	552.0	138.01	59.60	0.000	
A^2	1	6.0	6.02	2.60	0.129	not significant
B^2	1	87.6	87.56	37.81	0.000	
C^2	1	437.3	437.35	188.86	0.000	
D^2	1	20.5	20.48	8.84	0.010	
2-way Interaction	6	10185.9	1697.65	733.10	0.000	
AB	1	2835.6	2835.56	1224.48	0.000	
AC	1	3164.1	3164.06	1366.34	0.000	
AD	1	1580.1	1580.06	682.32	0.000	
BC	1	1914.1	1914.06	682.32	0.000	
BD	1	689.1	689.06	297.56	0.000	
CD	1	3.1	3.06	1.32	0.269	not significant
Error	14	32.4	2.32			
Lack-of-Fit	10	21.7	2.17	0.81	0.645	not significant
Pure Error	4	10.8	2.69			
Total	29	18444.8				
Model summary	S	R-sq	R-sq (adj)	R-sq (pred)		
	1.52175	99.82%	99.64%	98.74%		

Tables 4 and 5 also present the measures of R^2 (adequacy, adjusted, and predicted) and which is approximately equal to 1. All adequacy measures of R^2 are approximately equal to 1 indicating adequate models. The P-value for models

shown in Tables 4 and 5 that are less than 5% indicates more significant parameters with the rest deemed not significant. Based on the F-value, graphite content is noticeably the most dominant parameter among all the parameters that are influencing cutting forces and surface roughness.

Table 5. Analysis of Variance (ANOVA) of surface roughness.

Source	Degrees of freedom	Adj SS	Adj MS	F-Value	P-Value	Note
Model	15	1.88459	0.125639	129.34	0.000	significant
Blocks	1	0.01887	0.018873	19.43	0.001	
Linear	4	1.25102	0.312756	321.98	0.000	
A	1	0.00014	0.000139	0.14	0.711	not significant
B	1	0.30212	0.302123	311.03	0.000	
C	1	0.03300	0.033004	33.98	0.000	
D	1	0.91576	0.9157556	942.76	0.000	
Square	4	0.11068	0.027671	28.49	0.000	
A^2	1	0.01235	0.012354	12.72	0.003	
B^2	1	0.05405	0.054054	55.65	0.000	
C^2	1	0.01178	0.011778	12.12	0.004	
D^2	1	0.01438	0.014384	14.81	0.002	
2-way Interaction	6	0.35489	0.059148	60.89	0.000	
AB	1	0.08266	0.082656	85.09	0.000	
AC	1	0.12426	0.124256	127.92	0.000	
AD	1	0.06376	0.063756	65.64	0.000	
BC	1	0.00141	0.001406	1.45	0.249	not significant
BD	1	0.02641	0.026406	27.18	0.000	
CD	1	0.05641	0.056406	58.07	0.000	
Error	14	0.01360	0.000971			
Lack-of-Fit	10	0.00567	0.000567	0.29	0.951	not significant
Pure Error	4	0.00792	0.001981			
Total	29	1.89819				
Model Summary	S	R-sq	R-sq(adj)	R-sq (pred)		
	0.0311666	99.28%	98.52%	96.84%		

Cutting Forces

Cutting force dependency on input parameters can be explored through the contour diagrams in Figure 6. It can be inferred that all the hybrid nanocomposite samples need low cutting forces when the operation is performed at high cutting speeds, low depth of cut and lower feed. A greater emphasis must be placed on the graphite content in the sample. It is observed that the high graphite concentrations reduced the cutting forces required. Cutting forces are lower at high cutting speeds due to the thermal softening effect on the workpiece. It can be noticed that lower cutting forces are the result of maintaining the cutting speeds between the range of 50 to 100 m/min. At a lower depth of cut and low feed rate, the material removal rate is low which requires lower cutting energy thereby, making it consume less force for machining. The contour plots indicate that a rise in feed rate and depth of cut correspondingly increased the cutting force. This is because there is a higher material removal rate at higher feed rates which would demand more energy for machining operation and thereby increase the cutting force. The graphite content present in the given sample contributes to the efforts for regulating the cutting forces. It can be deduced that lower cutting forces are the result of high graphite content possessed by the given sample. The inherent low hardness of graphite reduced the strength of MMC thereby diminishing the machining energy requirements. These observations can be reconfirmed with the response plots in Figure 7 as well.

The microhardness of the resulting HNC has a direct relation with the graphite content in the materials. Though the microhardness of the HNCs is more than that of the base alloy, it exhibits a different trend when the analysis pertained to HNCs only. Increasing graphite content resulted in a subsequent decrease in microhardness [25]. Hence, cutting forces would also be reduced thereby making the material easily machinable. Graphite being a solid lubricant will act as a source of lubrication during the machining thus making the process more convenient with a reduction in cutting forces. Based on the above analysis, low cutting forces were obtained at a cutting speed of 96 m/min along with a depth of cut of 0.40 mm and feed rate of 0.05 mm / rev.

$$\begin{aligned}\text{Cutting force (CF)} = {} & 335.59 - 3.598\,A - 33.48\,B - 746.9\,C - 21.30\,D + 0.00225\,A^2 - 27.48\,B^2 + 2211\,C^2 \\ & - 2.594\,D^2 + 1.775\,A \times B + 11.250\,A \times C + 0.3975\,A \times D - 729.2\,B \times C - 21.87\,B \times D \\ & + 8.75\,C \times D\end{aligned} \quad (1)$$

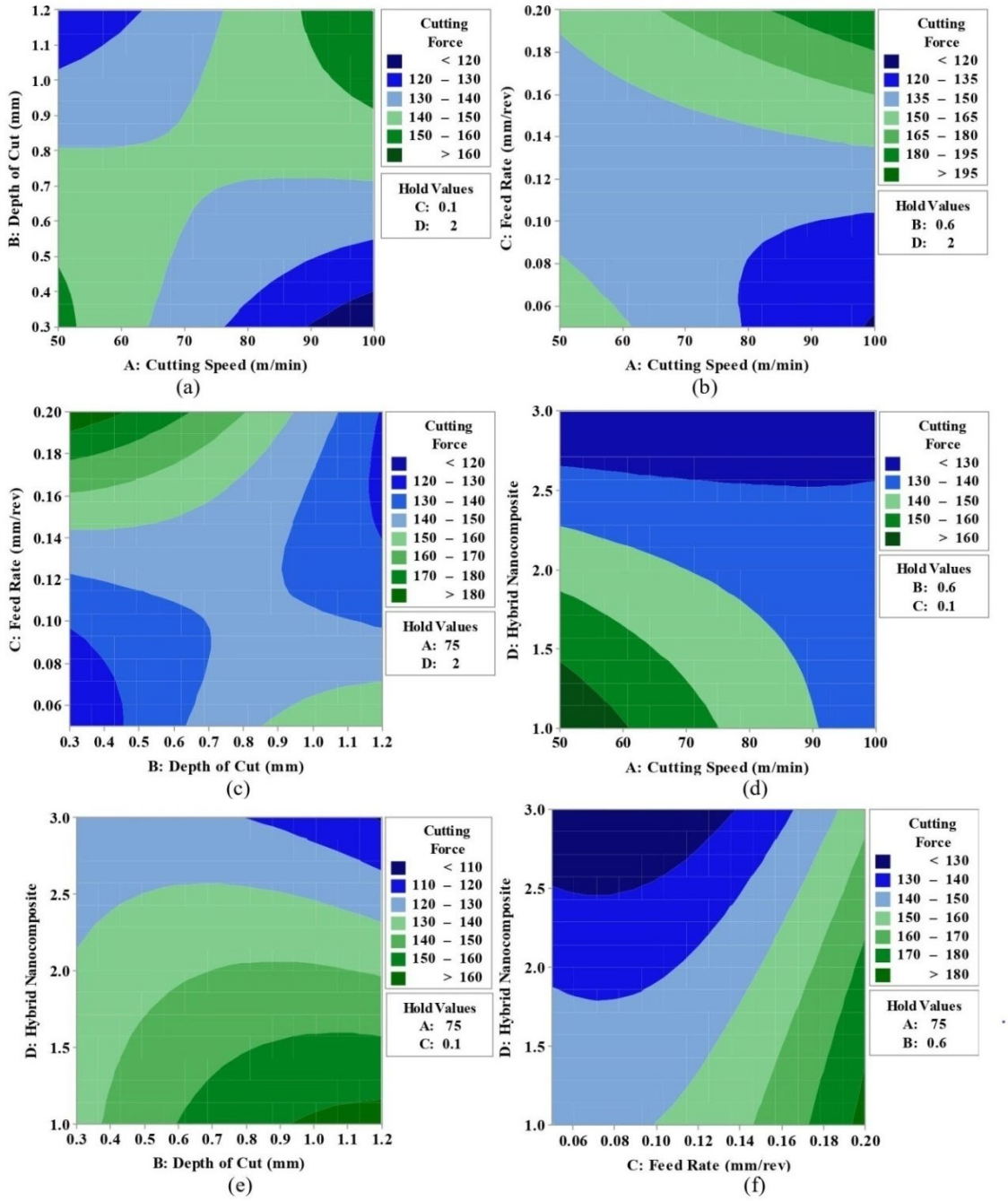

Figure 6. Effect of various input parameters on cutting force: (a) effect of depth of cut and cutting speed, (b) effect of feed rate and cutting speed, (c) effect of feed rate and depth of cut, (d) effect of graphite and cutting speed, (e) effect of graphite and depth of cut and (f) effect of graphite and feed rate.

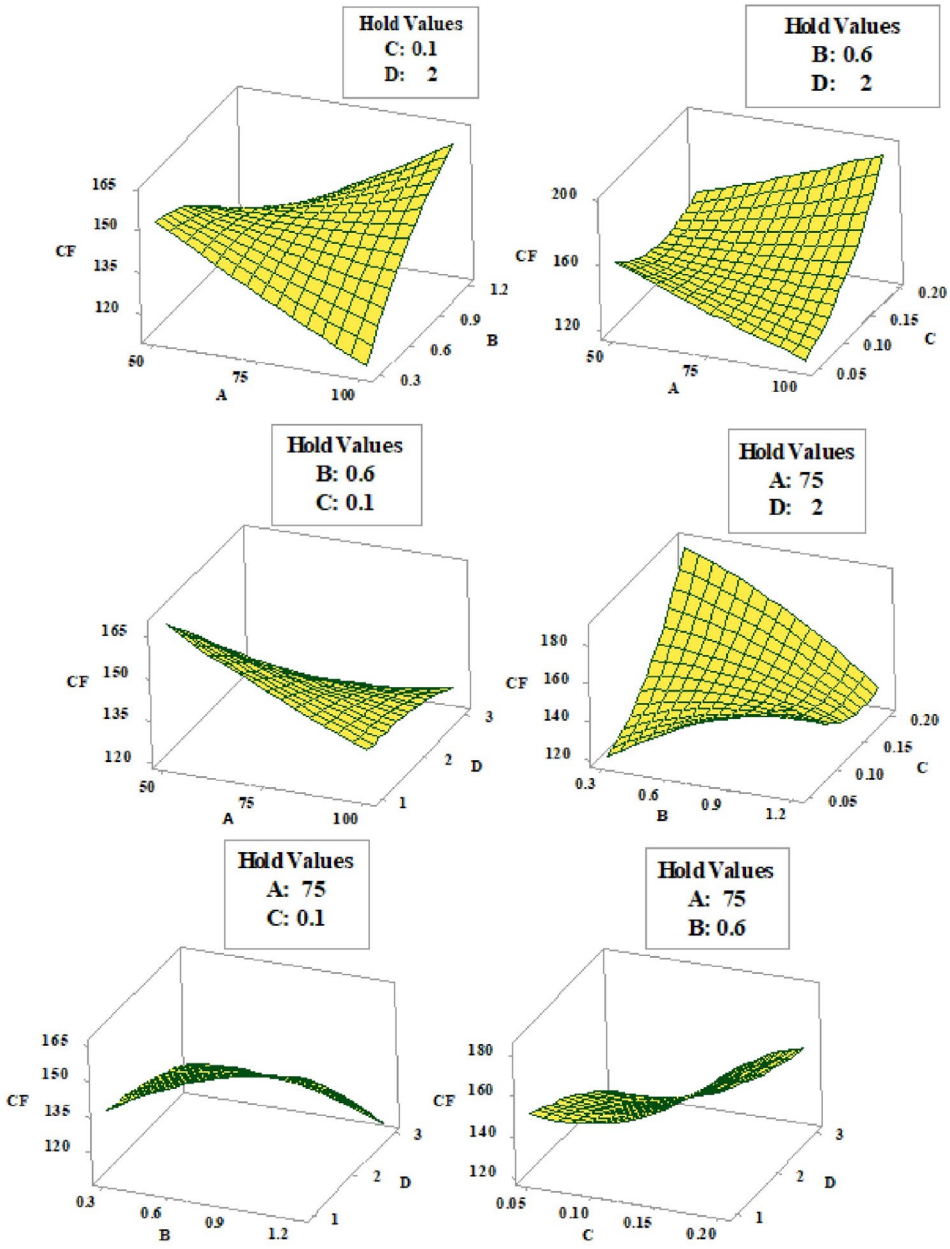

Figure 7. Response surface plot of cutting force.

Surface Roughness

Figure 8 represents the contour plots drawn concerning various parameters related to surface roughness. To minimize the surface roughness as much as possible, it becomes imperative that the machining must be performed with high cutting speeds but at low feeds and low depth of cuts. The other vital parameter i.e. graphite content in the material is crucial for regulating the surface roughness. Higher graphite concentrations would result in a smooth surface due to reduced surface roughness. Maintaining high cutting speeds would result in lower surface roughness due to the lower coefficient of friction [10]. The chances of built-up edge formation are low at high speeds thereby promoting a better surface finish. This observation is a well established fact concerning the built-up edge formation in the case of every machining operation. However, the ANOVA result for surface roughness from the present experimental results conveys that graphite content is more significant than cutting speed. This can be evidently seen in the findings of the concerned ANOVA analysis. The best surface finish was obtained at a cutting speed above 92 m/min and a depth of cut of less than 0.45 mm. It can be summarized that the lower feed rate (<0.01 mm/rev) produces a smooth surface as the tool advancement into the workpiece would be minimal along with closer feed marks and thus leading to a superior finish. Figure 9 displays the corresponding response surface plots drawn for surface roughness. The observations from these plots seem to be in accordance with the above discussion.

ANOVA analysis reveals that the graphite content and depth of cut have more influence on the surface roughness than feed rates and cutting speeds. It was proven in previous studies that the surface roughness has been minimized with the use of high cutting speeds along with a rise in the solid lubricant content in the matrix [17]. The low surface roughness was obtained at a cutting speed of 97 m/min, depth of cut of 0.45 mm and feed rate of 0.06 mm / rev. From the final mathematical model analysis, the equation to predict the surface roughness is as follows:

$$\text{Surface roughness}(R_a) = 0.942 + 0.00733\,A - 0.777\,B - 0.153\,C + 0.4369\,D - 0.000101\,A^2 + 0.6843\,B^2 - 8.21\,C^2 - 0.0683\,D^2 + 0.00958\,A \times B + 0.07050\,A \times C - 0.002525\,A \times D - 0.625\,B \times C - 0.1354\,B \times D - 1.188\,C \times D \quad (2)$$

Considering the aforementioned discussions and the inputs from the various plotted graphs concerning both cutting force and surface roughness, the optimum parameters would be a cutting speed of 97 m/min in association with a 0.42 mm depth of cut and a feed rate of 0.05 mm /rev.

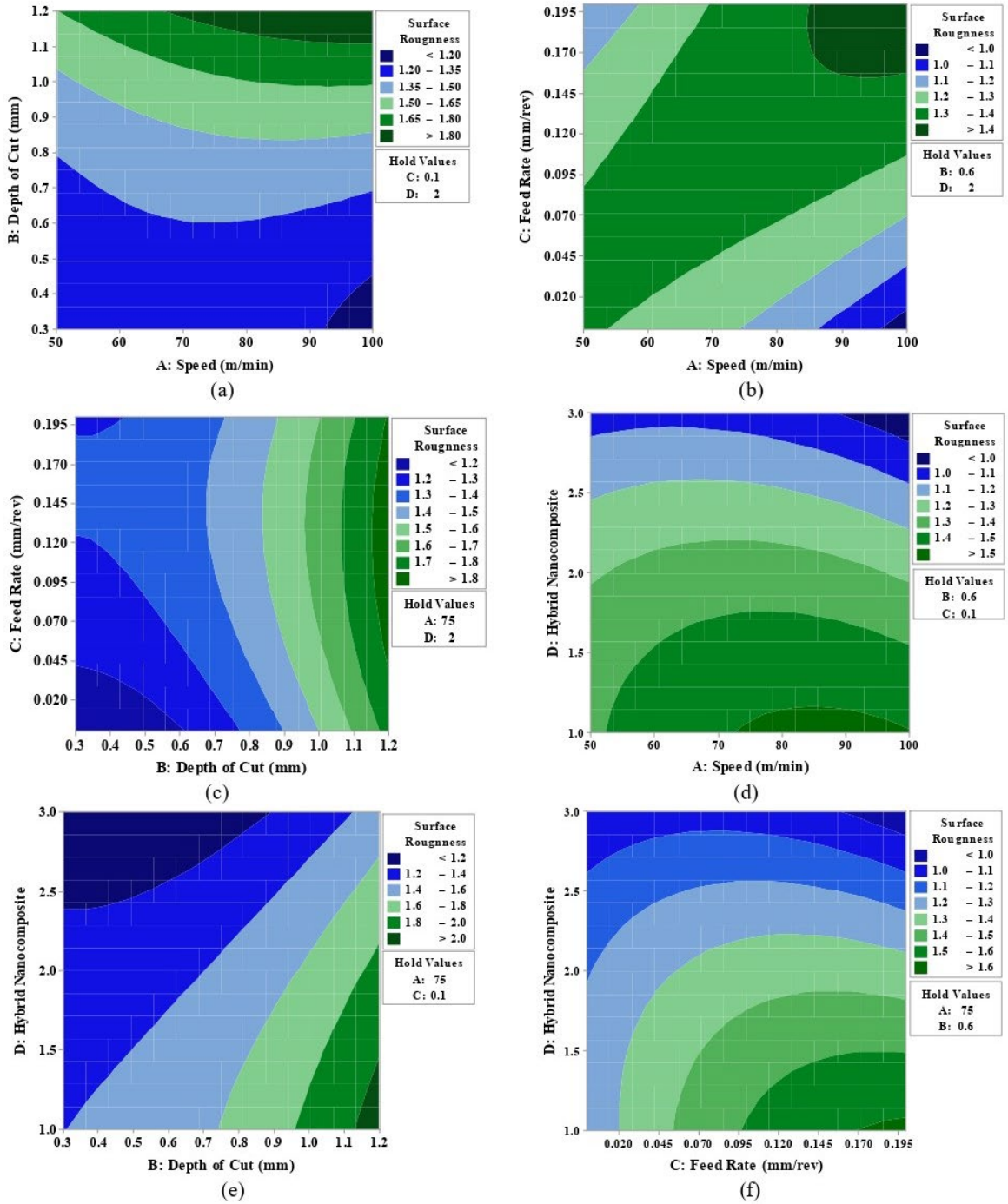

Figure 8. Effect of various input parameters on surface roughness: (a) effect of depth of cut and speed, (b) effect of feed rate and speed, (c) Effect of feed rate and depth of cut, (d) effect of graphite and speed, (e) effect of graphite and depth of cut and (f) effect of graphite and feed rate.

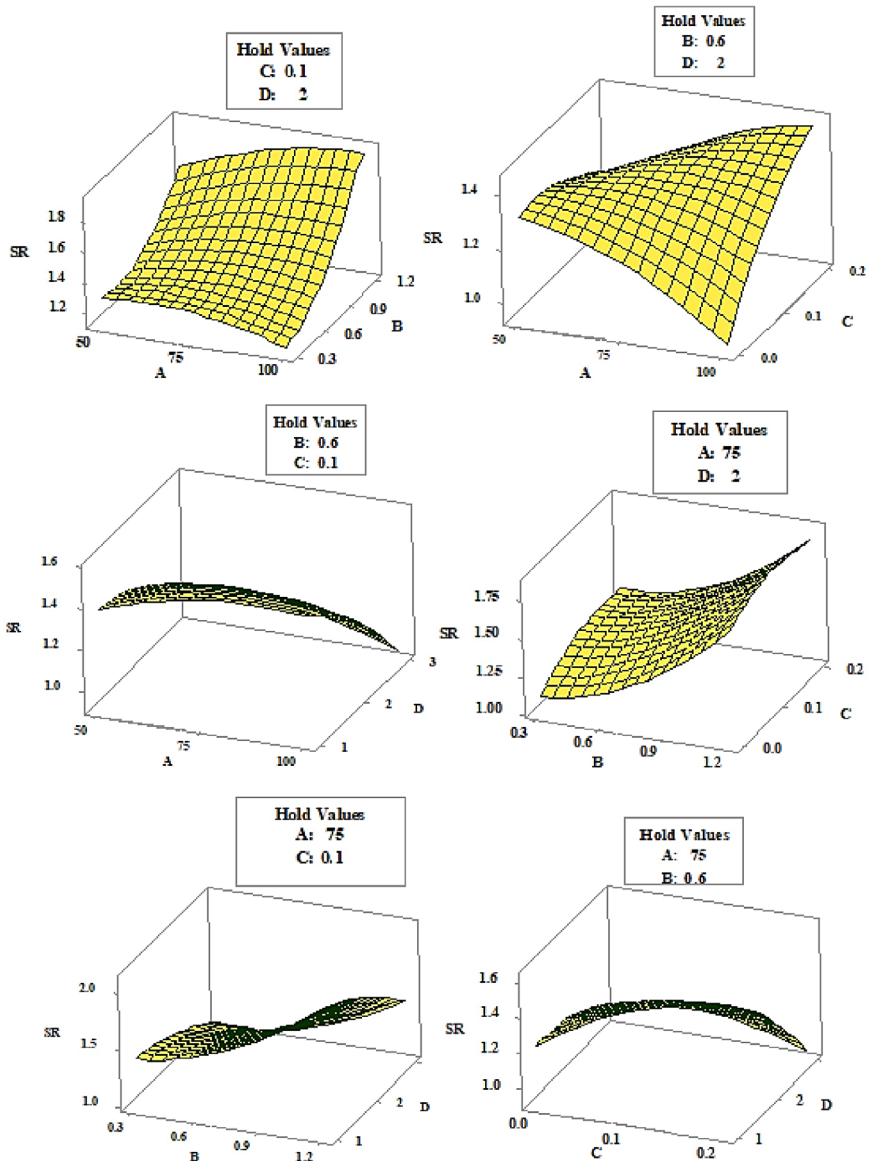

Figure 9. Response surface plot of surface roughness.

Chip Morphology

The formation of chips and their morphology are observed for all three HNC samples under the conditions of 100 m/min cutting speed, 0.05 mm/rev feed and 0.3 mm depth of cut. These conditions are selected based on the fact that high cutting speed coupled with low fed and low depth of cuts resulted in reduced cutting forces and better surface finish. To facilitate this task, SEM images of the chips were used to reveal the underlying aspects. Furthermore, chip composition was investigated for revealing their elemental composition in the form of weight and atomic percentages.

The SEM images for the chips obtained during the machining of 1HNC hybrid nanocomposites are displayed in Figure 10. It is noticed that the chips formed in a spiraling spring-type fashion indicating the formation of continuous chips. The high cutting velocity with a low feed rate resulted in the above chip condition. The formation of spring-type chips indicates a poor surface finish [18]. Sawtooth structures are absent in this chip. Such an observation can also be credited to the fact that worn out tools would also generate long and curly continuous chips without any saw tooth profile. The chip would still be in contact with the face of the tool for a while longer before its total departure from the workpiece. The free surface of the chip reveals the lamella structures on its topography. The surface of the chip contained stepwise facets on its sideways that are visible in the enlarged section of the free surface of the chip. From the EDX analysis, crests of carbon (C), magnesium (Mg), aluminium (Al), silicon (Si), and oxygen (O) are identified. Elemental analysis of the chip breaks down the composition into the above five constituents with aluminium and carbon as the major constituents. The rest of the constituents include Oxygen, Magnesium, and Silicon.

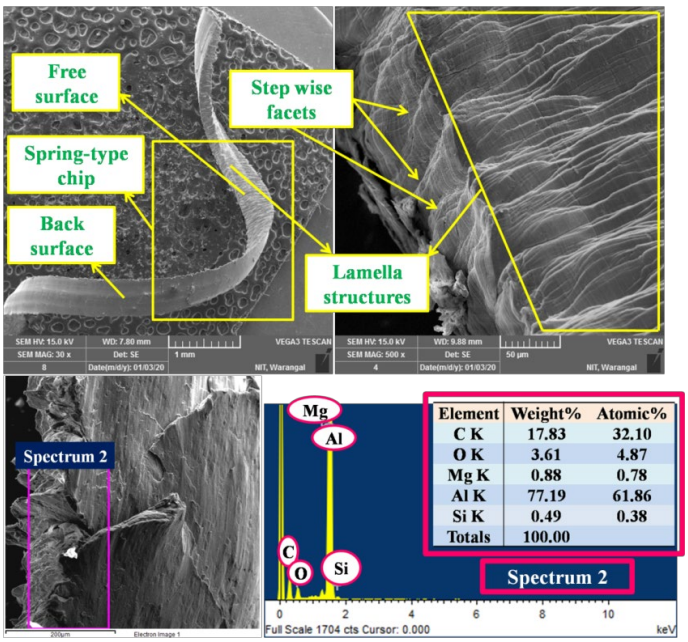

Figure 10. Chip morphology of AA6061-2SiCp-1 wt. % graphite hybrid nanocomposite.

Figure. 11 reveals the SEM image for the chips obtained while machining the 2HNC hybrid nanocomposite sample. Unlike the 1HNC sample, the chips obtained here are short and C-shaped. The back surface of the chip encountered some fractures in the form of cracks. It can also be observed that the chip also has a corrugated surface containing saw tooth structures on its periphery. The formation of saw-toothed chips can be credited to the diminishing ductility of the composite due to SiC and graphite addition [26]. The sawtooth formation is also regulated by cutting speed. The wear resistance of the 2 HNC is higher than that of the base alloy [10]. Sawtooth formation on the segmented chips is also an indication of a better surface finish [27]. While aluminium and carbon are still the major constituents, the elemental analysis showed that there was a decrement in the aluminium weight % relative to the 1HNC sample. This decrement has contributed to the rise in the composition of all other remaining constituents.

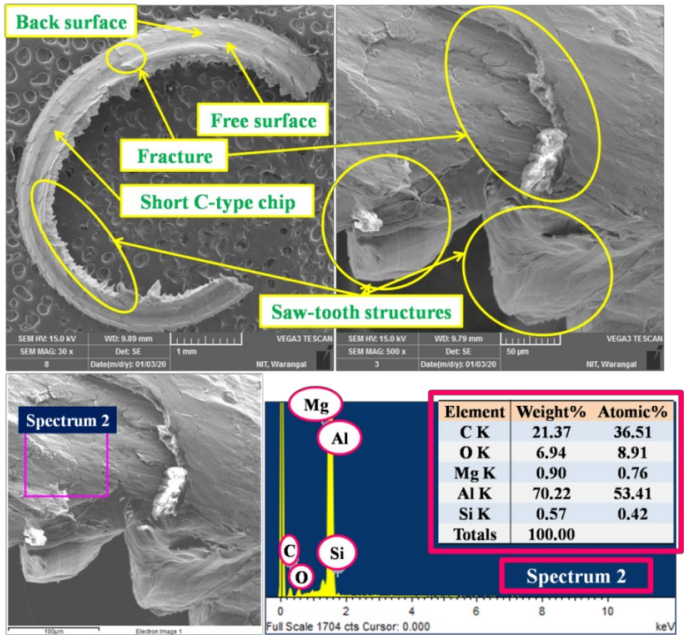

Figure 11. Chip morphology of AA6061-2SiCp-2 wt. % graphite hybrid nanocomposite.

The chip morphology of 3 HNC hybrid nanocomposite samples is displayed in Figure 12. The discontinuous chip consists of a fractured surface that can be better observed in the enlarged sections of the images. Crack propagation is also visible in the chip morphology along with the concerned elemental composition of the sample. Surface finish for this composition is even better than the rest of the samples, as evident from the previous sections. This can be reasoned with increased graphite presence which would further behave like a chip breaker and thereby reduce the surface roughness [28]. This sample being the one with the highest graphite content forms a thick graphite film which in turn limits the wear rate. Depletion in volumetric wear rates of the samples with the rise in graphite content would be linked to the dual-phase effect of SiCp and graphite nanoparticles in making a robust mechanically mixed layer (MML) over the surface of contact

[10]. The elemental analysis confirmed a trend of increments in weight of all other constituents at the expense of decreased aluminium content. Still aluminium and carbon grab the major chunks in the elemental composition of this sample. The existence of peak carbon intensity makes sure that the AA6061 aluminium alloy matrix undergoes as minimum as possible plastic deformation.

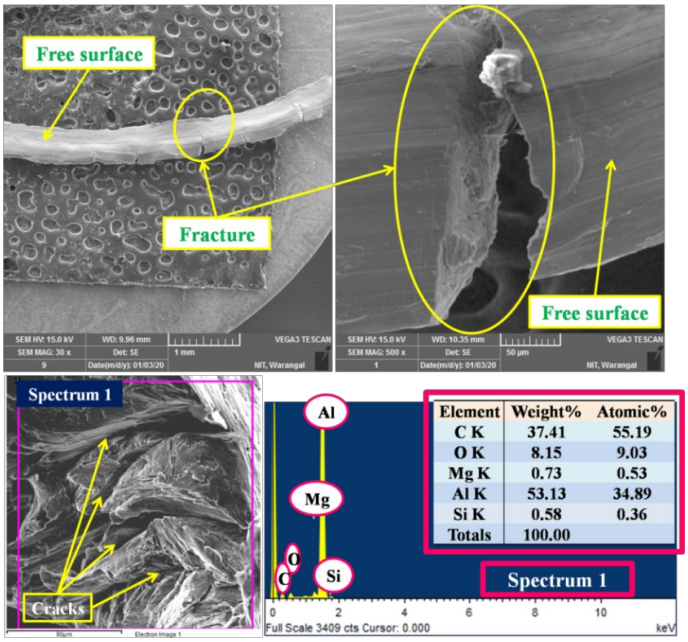

Figure 12. Chip morphology of AA6061-2SiCp-3 wt. % graphite hybrid nanocomposite.

CONCLUSION

The current study is aimed to understand the machinability of AA6061/2 wt.% SiC/ x wt.% graphite (x= 1, 2, 3) hybrid nanocomposites. A total of 30 experiments are done based on the experimental design by RSM with a three level approach and the corresponding output responses of cutting force and surface roughness are measured. Subsequently, ANOVA test is conducted separately on both the output responses at a 95% confidence level. The conclusions that emerged from this study are listed below:

i. Cutting force is reduced with the rise in cutting speed and graphite content at low feed rates and low depth of cuts.
ii. The increase of graphite content and cutting speed with low feed and depth of cut ensured low surface roughness.
iii. Graphite is the most notable parameter among all the others for both surface roughness and cutting force models.
iv. Optimized process parameters for obtaining a better surface finish and lower cutting forces include a cutting speed of 97 m/min with a 0.42 mm depth of cut and a feed rate of 0.05 mm/rev.
v. R^2 (adjusted) values for surface roughness and cutting force models are 98.52% and 99.64% respectively indicating that both models are a better fit for the analysis.
vi. Chip morphology studies on all the samples confirm that increased graphite presence would result in a superior surface finish due to the manifestation of a lubricating layer. Evidently, the sample with the highest graphite content possessed a better surface finish.

ACKNOWLEDGEMENT

The authors would like to thank the Director, NIT Warangal and the Department of Mechanical Engineering for their guidance and support in this research work. The authors would also confirm that this work received no specific grants from any agency in the public, commercial, or not-for-profit sectors.

REFERENCES

[1] A. Kareem *et al.*, "A review on AA 6061 metal matrix composites produced by stir casting," *Materials (Basel),* vol. 14, no. 1, pp. 1–22, 2021, doi: 10.3390/ma14010175.
[2] O. El-Kady and A. Fathy, "Effect of SiC particle size on the physical and mechanical properties of extruded Al matrix nanocomposites," *Mater. Des.*, vol. 54, pp. 348–353, 2014, doi: 10.1016/j.matdes.2013.08.049.
[3] C. Elanchezhian, B.Vijaya ramanth, G.B Bhaskar, M. Vivekanandhan, "An investigation of the mechanical properties of hybridcomposites in applications of automotive industry," *Mater. Today Proc.*, vol. 16, part 2, pp. 875-882, 2019, doi: 10.1016/j.matpr.2019.05.172.
[4] N.V. Babu and T. V. Moorthy, "Synthesis and characterization of Al7075/SiC composite by stir casting," *Appl. Mech. Mater.*, vol. 592–594, pp. 760–764, 2014, doi: 10.4028/www.scientific.net/AMM.592-594.760.

[5] P. Yadav *et al.*, "A contemporary review of aluminium MMC developed through stir-casting route," *Materials (Basel).*, vol. 14, pp. 1–30, 2021, doi: 10.3390/ma14216386.

[6] K.S.L. Narayana, M.M. Benal and H.K. Shivanand, "Effect of graphite on aluminium matrix composites fabricated by stir casting route - A review," *Mater. Today Proc.*, vol. 45, pp. 327–331, 2021, doi: 10.1016/j.matpr.2020.11.051.

[7] C. Kannan and R. Ramanujam, "Comparative study on the mechanical and microstructural characterization of AA 7075 nano and hybrid nanocomposites produced by stir and squeeze casting," *J. Adv. Res.*, vol. 8, part 4, pp. 309- 319, 2017, doi: 10.1016/j.jare.2017.02.005.

[8] A.P. Reddy, P.V. Krishna and R.N. Rao,"Dry sliding wear behaviour of ultrasonically-processed AA6061/SiCp nanocomposites," *Int. J. Automot. Mech*, vol. 14, no. 4, pp. 4747- 4768, 2017, doi: 10.15282/ijame.14.4.2017.12.0373.

[9] A. Sridhar, K.P. Lakshmi, "Evaluation of mechanical and wear properties of aluminum 7075 alloy hybrid nanocomposites with the additions of SiC/Graphite," *Mater. Today Proc.*, vol. 44, no. 1, pp. 2653-2657, 2021, doi: 10.1016/j.matpr.2020.12.675.

[10] A. Prasad Reddy, P. Vamsi Krishna and R.N. Rao, "Tribological behaviour of Al6061–2SiC-xGr hybrid metal matrix nanocomposites fabricated through ultrasonically assisted stir casting technique," *Silicon,* vol. 11, no. 6, pp. 2853–2871, 2019, doi: 10.1007/s12633-019-0072-9.

[11] P. Senthilkumar *et al.*, "Investigational studies on wear and machining properties of hybrid aluminium composites," *Mater. Today Proc.*, 2021, doi: 10.1016/j.matpr.2021.03.371.

[12] J.P.Chen, L. Gu and G.J He, "A review on conventional and nonconventional machining of SiC particle-reinforced aluminium matrix composites," *Adv. Manuf.* vol. 8, pp. 279–315, 2020, doi: 10.1007/s40436-020-00313-2.

[13] T. Ozben, E. Kilickap and O. Çakır, "Investigation of mechanical and machinability properties of SiC particle reinforced Al-MMC," *J. Mater. Process. Technol.*, vol. 198, no. 1–3, pp. 220-225, 2008, doi: 10.1016/j.jmatprotec.2007.06.082.

[14] H.K. Garg, K. Verma, A. Manna and R. Kumar, "Hybrid metal matrix composites and further improvement in their machinability- A review," *International Journal of Latest Research in Science and Technology*, vol. 1, no. 1, pp 36-44 , 2012.

[15] S. Deshmukh, G. Joshi, A. Ingle and D. Thakur, "An overview of aluminium matrix composites: Particulate reinforcements, manufacturing, modelling and machining," *Mater. Today Proc.*, vol. 46, no. 17, pp. 8410-8416, 2021, doi: 10.1016/j.matpr.2021.03.450.

[16] K. Venkatesan *et al.*, "Study of cutting force and surface roughness in machining of Al alloy hybrid composite and optimized using response surface methodology," *Procedia Eng.*, vol. 97, pp. 677-686, 2014, doi:10.1016/j.proeng.2014.12.297.

[17] A. Kannan, R. Mohan, R. Viswanathan and N. Sivashankar, "Experimental investigation on surface roughness, tool wear and cutting force in turning of hybrid (Al7075 + SiC + Gr) metal matrix composites," *J. Mater. Res. Technol.*, vol. 9, no. 6, pp. 16529-16540, 2020, doi: 10.1016/j.jmrt.2020.11.074.

[18] J. Suthar and K. Patel, "Tool wear and chip formation analysis of aluminium hybrid metal matrix composite," *Mater. Today Proc.*, vol. 32, no. 3, pp. 422-430, 2020, doi: 10.1016/j.matpr.2020.02.126.

[19] R. Angiras and O. S. Bhatia, "Analysis of surface roughness during turning operation of Aluminium-6063 using Taguchi approach," *Int. J. Adv. Res. Sci. Eng.*, vol. 4, no. 6,.

[20] E. Kilickap, "Modeling and optimization of burr height in drilling of Al-7075 using Taguchi method and response surface methodology," *Int. J. Adv. Manuf. Technol.*, vol. 49, no. 9–12, pp. 911–923, 2010, doi: 10.1007/s00170-009-2469-x.

[21] A. A. Thakre and S. Soni, "Modeling of burr size in drilling of aluminum silicon carbide composites using response surface methodology," *Eng. Sci. Technol. an Int. J.*, vol. 19, no. 3, pp. 1199–1205, 2016, doi: 10.1016/j.jestch.2016.02.007.

[22] T. Rajmohan and K. Palanikumar, "Application of the central composite design in optimization of machining parameters in drilling hybrid metal matrix composites", *Meas. J. Int. Meas. Confed.*, vol. 46, no. 4, pp. 1470-1481, 2013, doi: 10.1016/j.measurement.2012.11.034.

[23] D. Svetlizky et al., "The influence of laser directed energy deposition (DED) processing parameters for Al5083 studied by central composite design", *J. Mater. Res. Tech*., vol. 17, pp. 3157-3171, 2022, doi: 10.1016/j.jmrt.2022.02.042.

[24] A. Prasad Reddy, P. Vamsi Krishna and R.N. Rao, "Two-body abrasive wear behaviour of AA6061-2SiC-2Gr hybrid nanocomposite fabricated through ultrasonically assisted stir casting," *J. Compos. Mater.*, vol. 53, no. 15, pp.2165-2180, 2019, doi: 10.1177/0021998318822723.

[25] A.P. Reddy, P.V. Krishna and R.N. Rao, "Strengthening and mechanical properties of SiC and graphite reinforced Al6061 hybrid nanocomposites processed through ultrasonically assisted casting technique," *Trans. Indian Inst. Met.*, vol. 72, no. 9, pp. 2533–2546, doi: 10.1007/s12666-019-01723-y.

[26] S. Basavarajappa and J.P. Davim, "Influence of graphite particles on surface roughness and chip formation studies in turning metal matrix composites," *Mater. Res.*, vol. 16, no. 5, pp. 990-996, 2013, doi: 10.1590/S1516-14392013005000098.

[27] N. Radhika, R. Subramanian and A. Sajith, "Analysis of chip formation in machining aluminium hybrid composites," *E3 J. Sci. Res*, vol. 2, no. 1, pp. 009-015, 2014.

[28] M.T. Hayajneh, A.M. Hassan and M.AH. Al-Omari, "The effect of graphite particles addition on the surface finish of machined Al-4 Wt.% Mg alloys," *J. Mater. Eng. Perform.,* vol. 10, no. 5, pp. 521–525, 2001, doi: 10.1361/105994901770344656.